TSINGHUA SCIENCE AND TECHNOLOGY
ISSN 1007-0214 01/16 pp443–454
DOI: 10.26599/TST.2021.9010061
Volume 27, Number 3, June 2022

Developments and Applications of Tunneling Magnetoresistance Sensors

Shaohua Yan, Zitong Zhou, Yaodi Yang, Qunwen Leng*, and Weisheng Zhao*

Abstract: Magnetic sensors based on tunneling magnetoresistance (TMR) effect exhibit high sensitivity, small size, and low power consumption. They have gained a lot of attention and have potential applications in various domains. This study first introduces the development history and basic principles of TMR sensors. Then, a comprehensive description of TMR sensors linearization and Wheatstone bridge configuration is presented. Two key performance parameters, the field sensitivity and noise mechanisms, are considered. Finally, the emerging applications of TMR sensors are discussed.

Key words: tunneling magnetoresistance (TMR) sensor; linearization; Wheatstone bridge configuration; noise

1 Introduction

The sensor market is experiencing rapid growth in recent years, driven by the Internet of Things (IoT). Sensors of various types are employed in multiple domains to sense and collect data, assisting in improving the production efficiency and facilitating our lives. Magnetic sensors, for example, acccout for approximately 10% of the smart sensor market for IoT industries[1]. They are commonly used to detect the geomagnetic field for navigation and the tiny magnetic field generated by cerebral activity for medical diagnosis, or monitor the current in the power grid and electric vehicles.

Various advanced magnetic sensing technologies have materialized over the last decades, mainly including the Hall effect, the anisotropic magnetoresistance (AMR) effect, the giant magnetoresistance (GMR) effect, and the tunneling magnetoresistance (TMR) effect. Figure 1 demontrates the structures and principles of sensors that adopted the above-mentioned techniques. The Hall sensor has long enjoyed considerable market owing to its well-developed and low-cost production. However, the silicon-based Hall sensor has limited output, low accuracy, and large offset. Some techniques such as integrated magnetic flux concentrator (MFC) and chopper stabilization have been employed in Hall sensor to improve its performance[2], but it increases the power consumption. Thus, the adoption of the Hall sensor in emerging technologies is still a chanllege. Therefore, engineers are looking for a smart sensor solution with higher sensitivity, lower power consumption, smaller size, and more stable performance.

Magnetoresistance sensors first appeared in the market in the late 1990s. The AMR effect was experimentally discovered in 1856[3] and was firstly used as a transducer for reading magnetically recorded tapes in 1971[4]. Based on AMR effect, Honeywell designed the magnetic random-access memory (MRAM)[5]. The AMR sensor can also be used as a compass to measure the Earth's magnetic field. Although several semiconductor suppliers offer a range of commercially available devices, the AMR sensor's magnetoresistance (MR) ratio is usually less than 5%, limiting its further applicability. Conventional AMR sensor requires additional circuits or permanent magnets to reset the magnetization of the thin film after usage, which complicates packaging and raises the cost[6].

The GMR effect was independently discovered in

• Shaohua Yan, Zitong Zhou, and Weisheng Zhao are with the School of Integrated Circuit Science and Engineering, Beihang University, Beijing 100191, China. E-mail: yanshaohua@buaa.edu.cn; zzt0807@buaa.edu.cn; weisheng.zhao@buaa.edu.cn.
• Yaodi Yang and Qunwen Leng are with Beihang-Goertek Joint Microelectronics Institute, Qingdao Research Institute of Beihang University, Qingdao 266100, China. E-mail: yaodi.yang@mail.utoronto.ca; qunwen.leng@goertekusa.com.
* To whom correspondence should be addressed.
Manuscript received: 2021-02-27; revised: 2021-06-30; accepted: 2021-08-04

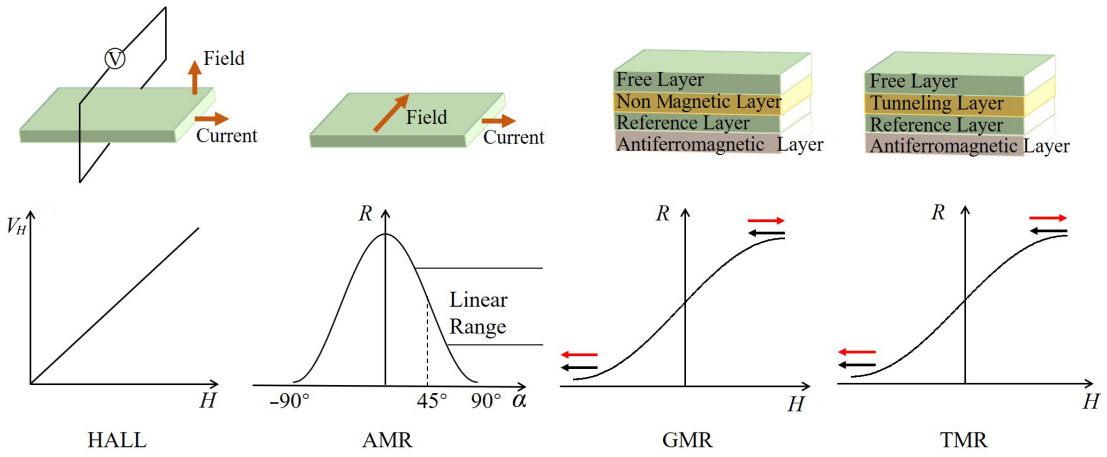

Fig. 1 Structures and principles of different magnetic sensors. V_H is the Hall voltage, H is the external magnetic field, R is the resistance of the device, and α is the angle between the current and the field.

1988[7, 8]. With the advent of spin valve structure[9], GMR sensors were quickly used as magnetic read head in the hard disk drive by IBM, resulting in higher storage capacities. The MR ratio in the metallic spin valve structure is typically around 10%.

The TMR effect at room temperature was first reported in 1995[10]. The MR ratio can reach more than 200% in CoFeB/MgO/CoFeB magnetic tunneling junction (MTJ)[11] and it is larger than other MR technologies. As shown in Table 1, TMR sensors have significant performance advantages. They are expected to become the new go-to solution for advanced precision, consistency, high sensitivity, low power consumption, and tiny package size required for tomorrow's advanced devices[12].

This study will firstly introduce the TMR sensor's working principles. The methods for linearization of MTJ and the implementation of Wheatstone bridge architecture are summarized. The key sensor performance parameters are then investigated. Finally, the TMR sensor's applications in different domains are discussed.

2 Design and Fabrication of TMR Sensors

A TMR sensor comprises MTJ elements. Figure 2

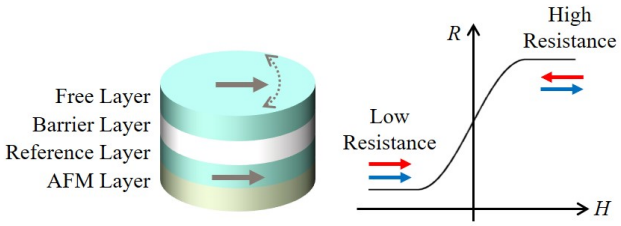

Fig. 2 Structure and *R-H* curve of the linear MTJ.

depicts the structural schematic of an MTJ. It is a thin-film stack composed of a sandwiched structure with a free layer (FL), a barrier layer, and a reference layer (RL). The RL's magnetization direction is fixed by an antiferromagnetic (AFM) layer, while the FL's magnetization direction can rotate under an external magnetic field. Equation (1) shows the resistance of the MTJ variation with the angle θ between the magnetization directions of the FL and RL.

$$R(\theta) = R_{\mathrm{p}} + \frac{(R_{\mathrm{ap}} - R_{\mathrm{p}})(1 - \cos\theta)}{2} \tag{1}$$

where R_{p} and R_{ap} are the resistance for parallel and antiparallel alignment of the ferromagnetic layers, respectively.

2.1 Linear strategies of MTJ

When used as a magnetic sensor, the MTJ must have a linear and free of hysteresis response to the external

Table 1 Comparison of magnetic sensing technologies.

Parameter	Hall	AMR	GMR	TMR
Sensing direction	Perpendicular	In-plane	In-plane	In-plane/Perpendicular
Sensitivity (mV/(V·Oe))	~0.05	~1	~3	~100
Power consumption (mA)	5~10	1~10	1~10	0.001~0.01
Size	Large	Medium	Medium	Small
Temperature stability (℃)	<150	<150	~300	~350
Linear range (Oe)	>10 000	~10	~100	~1000
Detectivity (nT/Hz$^{1/2}$)	>100	~1	~10	~0.01

field, necessitating the FL and RL magnetizations to be initially orthogonal[13]. Several methods for achieving a linearized output have been reported, as summarized in Fig. 3.

For example, in Fig. 3a, a pair of permanent magnets is integrated near the FL to generate a bias magnetic field perpendicular to the sensing direction of the MTJ[14]. It can help achieve a linear output while also stabilizing the FL's magnetization state. However, this method increases the production complexity and cost, which is incompatible with device miniaturization. Alternatively, shape anisotropy can be tailored to generate a proper self-demagnetizing field, as Fig.3b decipts, the MTJ is patterned into a rectangular shape, with its length orthogonal to the fixed magnetic direction[15]. In addition, when the free layer is thin enough, the material exhibits a superparamagnetic-like behavior, resulting in a no-hysteresis loop[16]. But this method will significantly reduce the MTJ's sensitivity and increase its noise level. The fourth method involves adding an exchange bias layer to the free layer, as illustrated in Fig. 3c. The two antiferromagnetic layers have different blocking temperatures. Upon annealing process, it is possible to set the orthogonal magnetizations of FL and RL[17].

The above linearization methods are usually applied in the MTJ with in-plane magnetic anisotropy. For the MTJs sensing the perpendicular magnetic field, a more concise approach is to employ an in-plane magnetized free layer and a perpendicular magnetized reference layer[18], as shown in Fig. 3d. In this kind of structure, as the thickness of the free layer is carefully chosen, the magnetic moment can rotate from in-plane to out-of-plane, which gives a no-hysteresis output. Recently, another method for achieving linearization by tuning the MgO capping layer thickness in MTJ with double CoFeB/MgO interface structure has been reported[19], where a small linear range and a large sensitivity can be attained.

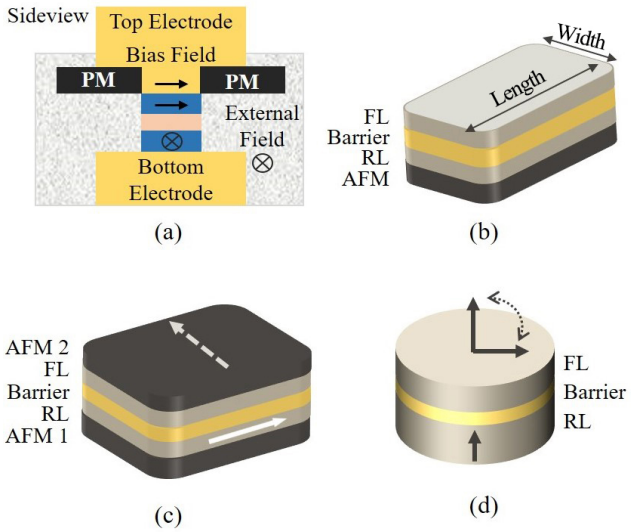

Fig. 3 Schematics of linearization methods in MTJ: (a) Intergration with permanent magnets; (b) shape anisotropy; (c) soft-pinned free layer; and (d) crossed-pattern magnetization.

2.2 Wheatstone bridge configuration

A single MTJ cannot be employed directly as a magnetic sensor, because the resistance of the MTJ varies with temperature[20]. The MTJs are usually arranged into the Wheatstone bridge configuration to prevent the thermal drift and improve the stability of sensors in harsh environments. The bridge has no output when the resistances in the four bridge arms change uniformly with temperature. Figure 4 shows the different bridge configurations. V_b and V_o are the applied bias voltage and the output voltage, respectively. R_1, R_2, R_3, and R_4 are the resistances of the four bridge arms. The unique bridge, the half bridge, and the full bridge are divided according to the number of active resistors[21]. The inactive resistors in unique bridge and half bridge structures are usually shielded with soft magnetic materials like NiFe. The full bridge structure in Fig. 4 has the highest sensitivity and exhibits a linear output. It is the most suitable for applications, where the two adjacent bridge arms have opposite responses to the external magnetic field. This requires that the MTJs forming the bridge arms should have opposite magnetic pinning directions.

There are usually four methods forming a full Wheatstone bridge configuration, as Fig. 5 illustrates.

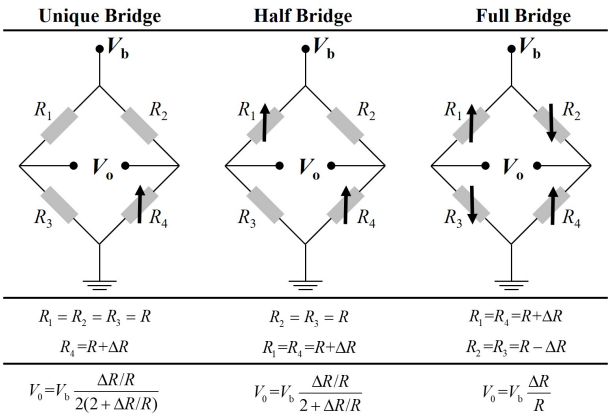

Fig. 4 Wheatstone bridge configurations for magnetic sensors.

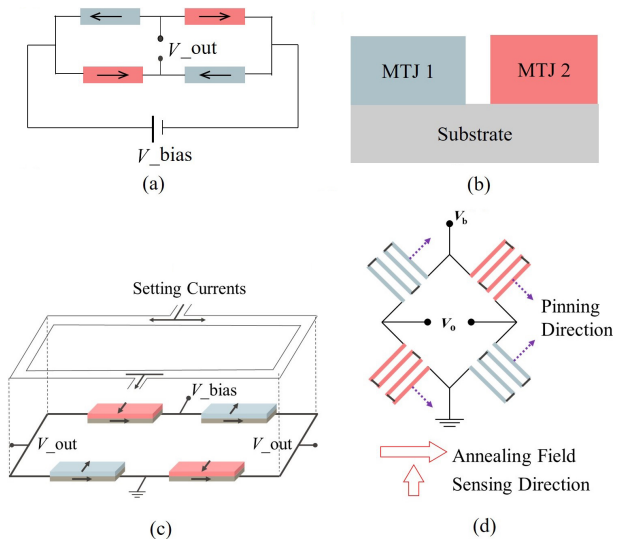

Fig. 5 Methods for fabricating a full-bridge TMR sensors: (a) Assembly of four identical resistors; (b) deposition of two film stacks on one wafer; (c) local annealing by current; and (d) one-time post annealing.

The simplest solution is to assemble the MTJs with opposite sensing directions. This method is always prone to alignment errors and is therefore unsuitable for mass production. As a result, a monolithic full-bridge sensor is more needed.

The second approach uses lithography to define different areas on the same wafer, then deposit thin films of different structures in each area. For example, an extra ferromagnetic layer is added to the "CoFe/Ru/CoFe" synthetic antiferromagnetic (SAF) structure to form a three-layered "CoFe/Ru/CoFe/Ru/CoFeB" structure. Due to antiferromagnetic coupling, the two structures' reference magnetizations will be pointing towards opposite directions under the same annealing condition[22]. The film can then be patterned directly into Wheatstone full-bridge sensors. This method simplifies the fabrication process, but it extremely complicates the film deposition. The two thin film structures also need to be designed precisely to ensure that they have similar magnetic properties (TMR ratio, RA product, and so on) to avoid output offset.

The third method is to set the pinning direction of the MTJs by local annealing. This is achieved by a current flow through the overlaid setting circuit to realign the RL magnetization[23]. As shown in Fig. 5c, the current flows in opposite directions for two pairs of resistors in the bridge. The current amplitude should be carefully calculated and a particular printed circuit board is required. A similar method uses laser radiation in an applied field in place of the setting circuit[24].

The fourth method is concise and compatible with mass production. The film is deposited and patterned based on a special layout, as shown in Fig. 5d. A post-annealing process is then performed. The pinning direction can be set along the patterned stripe's transverse orientation[25]. This method has been successfully used for the MR sensor production on 6-inch wafers[26].

The techniques mentioned above for fabricating a full Wheatstone bridge structure are primarily applicable for in-plane TMR sensors. In a perpendicular TMR sensor, an on-chip flux concentrator array is designed to bend the flux from the perpendicular direction into the in-plane direction enabling a full-bridge operation[27]. A more straightforward method should be explored further.

3 Critical Parameters of TMR Sensors

The detectivity of the TMR sensor is defined as

$$D=\frac{1}{S}\sqrt{\frac{S_V}{V^2}} \tag{2}$$

where S is the sensitivity of the sensors, V is the applied bias voltage, and S_V/V^2 is the normalized noise level. The value in $\mathrm{T/Hz^{1/2}}$ denotes the minimum magnetic field magnitude that the sensor could detect at a determined frequency. Owing to unremitting research efforts, the detectivity of 5 $\mathrm{pT/Hz^{1/2}}$ at 1 Hz is now realizable in TMR sensor[28], but it still falls short of other magnetic sensing technology such as superconducting quantum interference device (SQUID). Increased sensitivity and noise level suppression are required to imrove the detectivity further.

3.1 Sensitivity

Sensitivity is one of the critical performance parameters of TMR sensors. In the linear range of the sensor transfer curve, it is defined as

$$S=\frac{\mathrm{MR}}{2\mu_0 H_\mathrm{k}} \tag{3}$$

where MR and H_k are the MR ratio and the magnetic anisotropy field of the sensing layer, respectively. μ_0 is the vacuum permeability. Improving the sensitivity requires an increase in TMR ratio and reduction in H_k.

A large TMR ratio is usually achieved by optimizing the thin film materials. With previously used amorphous Al_2O_3 tunneling barrier, the TMR ratio of MTJ was only about 70% at room temperature[29]. After replacing the Al_2O_3 barrier with the crystalline MgO barrier, a significant increase in TMR ratio is realized thanks to the improved crystal perfection and orientation[30].

The TMR ratio is also found to be dependent on the composition and thickness of CoFeB ferromagnetic layer[31]. In addition, the half-metallic Heusler alloy with high spin polarization is advantageous as the ferromagnetic layer material[32]. Meanwhile, the device's magnetic properties can be influenced by its geometry. For example, because of the non-uniform magnetization state of the sensing layer, the TMR ratio may be greatly reduced as the device aspect ratio increases[17]. Therefore, there must be a compromise between the signal output and the linear response characteristics.

Controlling magnetic anisotropy in the free layer is quite crucial to obtain small H_k, which is usually realized by modifying the device geometry or using soft ferromagnetic materials.

Incorporating the sensors with MFCs is another method improving the sensitivity. Physical vapor deposition of materials with high magnetic permeability, such as CoZrNb and NiFe, is generally employed to prepare MFCs[33]. MFCs' primary function is to amplify the magnetic field to be measured; the gain in sensitivity is related to the shape and spacing of MFCs.

3.2 Noise

Theoretical and experimental noise analyses in MTJs have been studied extensively in recent years[34, 35]. Figure 6 reveals that noises in TMR sensors come from different mechanisms, and are classified as white noise and frequency-dependent noise. The white noise includes the thermal noise and the shot noise. The 1/f noise and the random telegraph noise (RTN) are frequency-dependent noise. Noises in TMR sensors can also be divided into magnetic noise and electrical noise. The magnetic noise is unique to magnetic materials and may have a dominant impact on the TMR sensors during operation. In addition to the intrinsic noises of the MTJ, the peripheral circuit and the environment

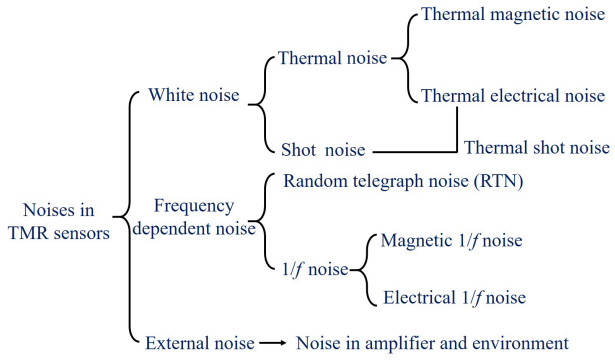

Fig. 6 Noises sources in TMR sensors.

noises should also be taken into account. The total noise can be regarded as the superposition of different noise components. The total noise power spectral density (PSD) (unit of T^2/Hz) is expressed in Eq. (4):

$$S_B = \left(\frac{dB}{dV}\right)^2 (S_V^{\text{therm-shot}} + S_V^{\text{elec-1/}f} + S^{\text{Amp}}) + S_B^{\text{therm-mag}} + S_B^{\text{mag-1/}f} \quad (4)$$

where $S_V^{\text{therm-shot}}$, $S_V^{\text{elec-1/}f}$, S^{Amp}, $S_B^{\text{therm-mag}}$, and $S_B^{\text{mag-1/f}}$ are thermal-shot noise, electronic 1/f noise, amplifier noise, thermal magneic noise, and magnetic 1/f noise, respectively. dV/dB is the sensitivity of sensor. The origin and suppression methods of noises in TMR sensors are discussed in this section.

3.2.1 Thermal noise

In TMR sensors, thermal noise is divided into thermal-electronic noise and thermal-magnetic noise. The thermal-electronic noise, also known as Johnson-Nyquist noise, mainly originates from the random motion of carriers near the Fermi surface affected by temperature. In 1928, Nyquist and Johnson proposed a computational model for thermal electronic noise[36, 37],

$$S_V^{\text{therm-elec}} = 4K_B RT \quad (5)$$

where $S_V^{\text{therm-elec}}$ denotes the PSD of this noise, K_B is the Boltzmann constant, and T is the ambient temperature. The thermal-electronic noise is only related to the resistance value and the ambient temperature.

Magnetization fluctuation caused by the magnetic field and thermal excitation is the primary source of the thermal-magnetic noise. According to some studies, thermal-magnetic noise originates from thermally excited domain walls hopping between magnetic layers and decreases with increasing of free layer volume[38, 39]. Based on the fluctuation-dissipation theorem (FDT), Egelhoff et al. gives its calculating model as[35]

$$S_B^{\text{therm-mag}} = \frac{4K_B T \mu_0 \alpha_G}{\Omega \gamma M_s} \quad (6)$$

where α_G is the Gilbert damping of the material, Ω is the free layer volume, γ is the gyromagnetic ratio for an electron, and M_s is the saturation magnetization intensity. Magnetic noise is probably the primary noise source during the TMR sensors operation, and its magnitude is considerably larger than that of the electrically generated noise[12].

3.2.2 Shot noise

Thermal effects and the stochastic nature of the electron emission process contribute to shot noise. The insulating barrier layer in the MTJ can be regarded as a

discontinuity where the shot noise is generated. Because the GMR sensor's film layers are all metallic, such noise is not observed. The shot noise's PSD is expressed as

$$S_V^{\text{shot}} = 2eIR^2 \tag{7}$$

where e is the electron charge, and I denotes the applied current. Considering the thermal effect when a current is applied in MTJs, a general expression for thermal-shot noise is given as

$$S_V^{\text{therm-shot}} = 2eIR^2 \coth\left(\frac{eV}{2K_BT}\right) \tag{8}$$

Equation (8) reveals that increasing the bias voltage on MTJ reduces the thermal-shot noise. However, increasing the bias voltage decreases the TMR ratio of the MTJ[40].

3.2.3 1/*f* noise

1/*f* noise is divided into electronic and magnetic 1/*f* noises in magnetic films. Charge trapping in the barrier or near the layer interface is the source of the electronic 1/*f* noise[41]. It can be calculated as

$$S_V^{\text{elec}-1/f} = \alpha_{\text{elec}}\frac{V^2}{Af} \tag{9}$$

where A is the sensing area of the MTJ, f is the frequency, and α_{elec} is the electric Hooge parameter, which is related to RA product, MR ratio, magnetization state, and the bias voltage[34, 42]. The 1/*f* noise becomes the most important noise source in the low frequency regime. As seen in Eq. (9), the electronic 1/*f* noise can be reduced by increasing the area of the free layer. This can be achieved by increasing the number of MTJs connected in series and parallel. As illustrated in Fig. 7, the 1/*f* noise can be theoretically reduced by an $M \times N$ factor by connecting N MTJs in series and then in parallel with M rows, while the total resistance can be adjusted to maintain a low thermal noise[43].

The modulation technique is an alternative approach to eliminate the electronic 1/*f* noise. MFCs are deposited on the microelectromechanical systems (MEMS) flaps

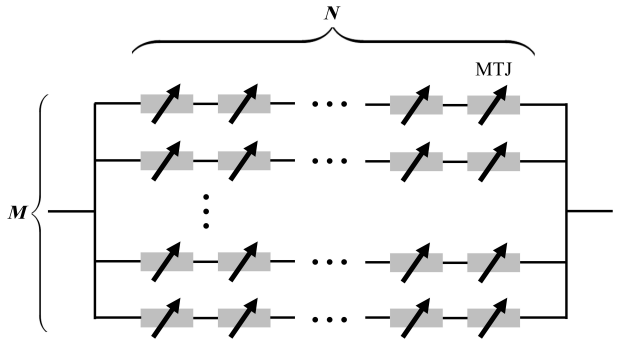

Fig. 7 MTJs connected in series and parallel.

that oscillate at very high frequencies driven by an electrostatic comb drive. The TMR sensor is placed in the middle of the flaps. The whole system shifts the operating point of sensor to the high frequency regime[44]. However, some technical challenges, such as the low modulation efficiency and high power consumption, need to be overcome.

The magnetic 1/*f* noise originates from the magnetization hopping between metastable ripple states. Egelhoff gives its PSD through the FDT as

$$S_B^{\text{mag}-1/f} = \frac{2B_{\text{sat}}\alpha_{\text{mag}}}{\Omega f} \tag{10}$$

where B_{sat} denotes the saturation field of the free layer and α_{mag} is the magnetic Hooge parameter.

Both thermal-magnetic noise and magnetic 1/*f* noise are magnetically derived noise. These noises are associated with the sensing layer volume and they can be reduced by increasing the sensing area or the thickness of the sensing layer according to Eq. (6) and Eq. (10). Using ultra-low Gilbert damping materials as ferromagnetic layer can also reduce the magnetic noise effectively[45]. A synthetic free layer structure has also been proposed, demonstrating the advantage of magnetic noise cancellation[46]. Alternatively, reducing the free-layer thickness can also minimize the saturation field. But a trade-off between the sensitivity and noise level needs to be reached. The method of voltage-induced anisotropy modulation is presented to mitigate the intrinsic noise without sacrificing TMR ratio[47].

3.2.4 Random telegraph noise

Random telegraph noise is discovered and proposed in the study on the field-effect transistors. RTN is not always evident. In TMR sensors, it is usually overshadowed by 1/*f* noise in the low-frequency regime. The RTN appears when the device size is small enough and in high frequency regime. It is expressed as

$$S_V^{\text{RTN}} = \frac{S_0}{1 + (f/f_0)^2} \tag{11}$$

where S_0 denotes the frequency-independent portion of the PSD, f_0 is the characteristic roll-off frequency described by $f_0 = (2\pi\tau)^{-1}$, and τ is the relaxation time of Lorentzian fluctuations.

4 Application

As a newly thriving technology, the TMR effect has been widely applied in the MRAM industry. Leading semiconductor suppliers have announced the release of embedded MRAM to replace eFlash or Dynamic Random Access Memory (DRAM)[48]. In the meantime,

the TMR sensor market has also seen a strong development in the past years. TMR sensors are likely to replace the AMR, GMR or traditional Hall sensors due to their higher output and signal to noise ratio, good compatibility with CMOS, and miniaturized size. Several examples are selected in this section to introduce the emerging applications of TMR sensors.

4.1 Biomedical detection

With improving detectivity, TMR sensors are becoming increasingly popular in biomedical applications. They are used to determine the presence or the concentration of target analyte molecules such as DNAs and proteins[49] labeled by magnetic nanoparticles (MNPs). TMR sensors exhibit lower background noise and are more robust than conventional optical biosensors[50].

Figure 8a shows a schematic of biodetection using TMR sensors. The surface of the TMR sensor is pre-coated with probe molecules to measure a specific target analyte. The probe molecules can capture the target molecules tagged by MNPs based on the specific binding of biomolecules. Then the underneath sensors can detect the fringe field generated by the magnetic labels. The concentration of the target analytes can be dertermined after quantitatively analyzing the signal. The integration of the TMR sensors and microfluid channels enables the realization of Lab-on-chip systems, which are promising in portable Point-of-Care devices.

Some research groups have demonstrated that the TMR sensors can also directly detect the generated magnetic field from the human heart or brain[51, 52]. Thus, magnetocardiography (MCG) and magnetoencephalography (MEG) have received much attention in recent years. These signals contain valuable information for medical diagnosis. Because the magnetic signal is not affected by the conductivity of human body, MCG and MEG present some advantages over electrocardiography (ECG) and electroencephalography (EEG), they have higher spatial and temporal resolution[53]. TMR sensors are less expensive and much smaller than the current SQUID technology used in MCG and MEG. The measurement must done in a magnetically shielded room, with the TMR sensor placed on the surface of the tested body, and the bio-magnetic field signal can be easily acquired using a low-noise amplifier circuit, as shown in Fig. 8b.

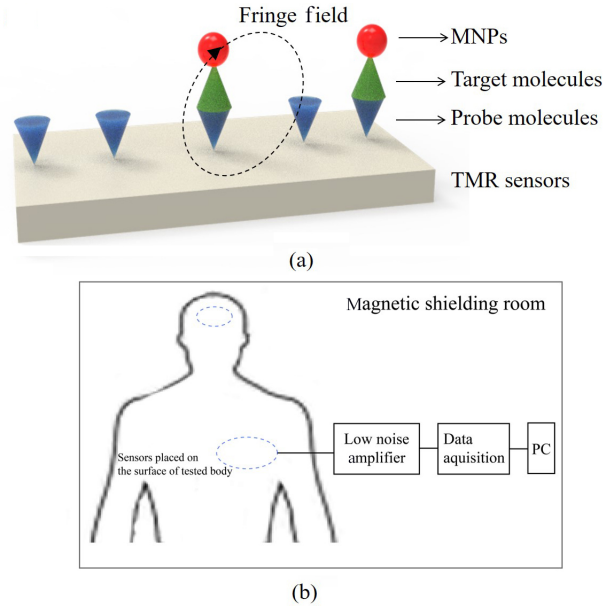

Fig. 8 Schematics for biodetections using TMR sensors: (a) molecules detection; (b) MCG and MEG.

TMR sensors on a flexible substrate were also developed recently[54, 55]. The TMR ratio can be preserved up to 190% regardless of the bending radius. The flexible magnetic sensors pave the way to realization for new applications such as human–computer interactions[56], electronic skins[57], and wearable devices[58].

4.2 Current sensing

Electrical current can be measured by sensing its emitted magnetic field. Based on this principle, the TMR sensor can be used to monitor the power consumption of household appliances[59]. Figure 9a shows the schematic of the TMR current sensor. Four identical TMR elements are connected into a Wheatstone bridge architecture. A U-shaped current line beneath the sensor creates opposite magnetic fields for two pairs of the bridge arms to obtain a full-bridge configuration. This sensor is integrated with signal processing units and real-time voltage sensor and can measure the active power delivered to the load from a 50/60 Hz AC line[60]. The TMR current sensor is a non-contact sensor that is easy to be installed without any service interruption. With the device miniaturization, the TMR sensor is also favorable in current sensing modules in the integrated circuits (IC).

The advantages of low cost and low power consumption of TMR sensors make them ideal candidates for large-scale current monitoring in the power grid. The traditional current transformers used in power systems have large sizes and limited frequency bandwidths. They are costly and require periodic maintenance. The TMR sensor arrays can be installed

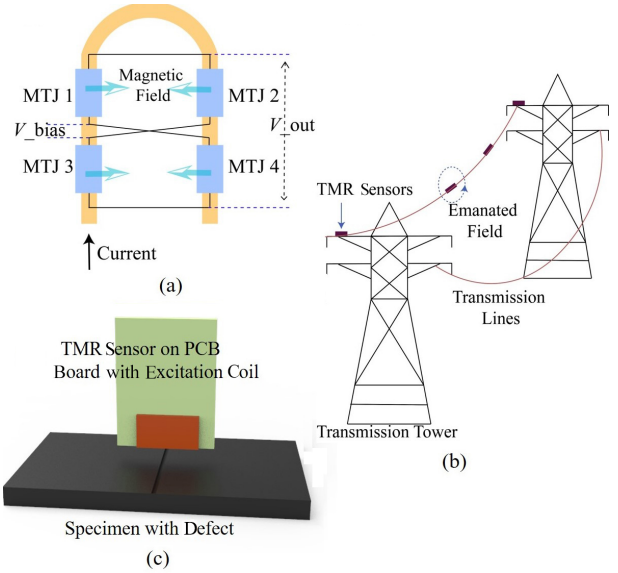

Fig. 9 Applications of TMR in current sensing: (a) U-shaped current line below a full-bridge sensor; (b) current monitoring in power transmission lines; and (c) NDT.

along the over-head transmission lines and underground distribution cables[61, 62], as Fig. 9b depicts. The information on the currents can be reconstructed and collected with high spatial resolution from the measured magnetic field signal, allowing for precise detection and accurate repair of abnormal points.

In non-destructive testing (NDT), eddy current sensing is widely used to detect defects on metal surfaces or ferromagnetic pipes. An excitation-detection probe for NDT is shown in Fig. 9c, which consists of an excitation coil that induces eddy current within the specimen and an array of TMR sensors that sense the resulting magnetic field[63]. The discontinuity in the generated field caused by defects in the specimen can be detected with this probe. The bandwidth of the TMR sensor is up to hundreds of MHz, which is much higher than the conventional pickup coils. A large-scale TMR senso array applied for magnetic field imaging (MFI) also contributes to improving the spatial resolution in NDT[64, 65].

4.3 Temperature monitoring

The temperature characteristics of MTJs can also be exploited in addition to detecting the magnetic field directly or indirectly[66]. With the transistor scaling down and more components integrated on a chip, temperature monitoring becomes a critical issue for ensuring the reliable operation of system-on-chip (SoC). The MTJs working as temperature sensor in SoC or IC have the advantages of compactness, lower energy consumption, and faster transit speed than the currently available thermal sensors, like Metal Oxide Semiconductor (MOS) transistor, ring-oscillator and so on.

One kind of nano temperature sensor has been proposed based on the stochastic switching behavior of MTJs [67]. As shown in Fig. 10a, an MTJ is set to antiparallel state as a reference resistor. An input current passes through the heavy metal underlayer of the other MTJ to realize a spin-orbit torque driven magnetization switching. The MTJ switches with a given probability depending on the operating temperature in the presence of thermal noise. The switching probability is determined from duplicating such measurement cycles to ensure the precision of temperature sensing. This kind of sensor can work for a linear temperature regime of 200 ∼ 400 K. When the number of measurement cycles is increased to 100 000, the corresponding conversion rate is 2500 samples per second, lowering the temperature sensing error to 1 K, while consuming less than 10 nJ of energy. Although the MTJ's probabilistic switching is often seen as a disadvantage in memory application, the MTJ-enabled on-chip temperature sensor outperforms the state-of-the-art CMOS temperature sensors.

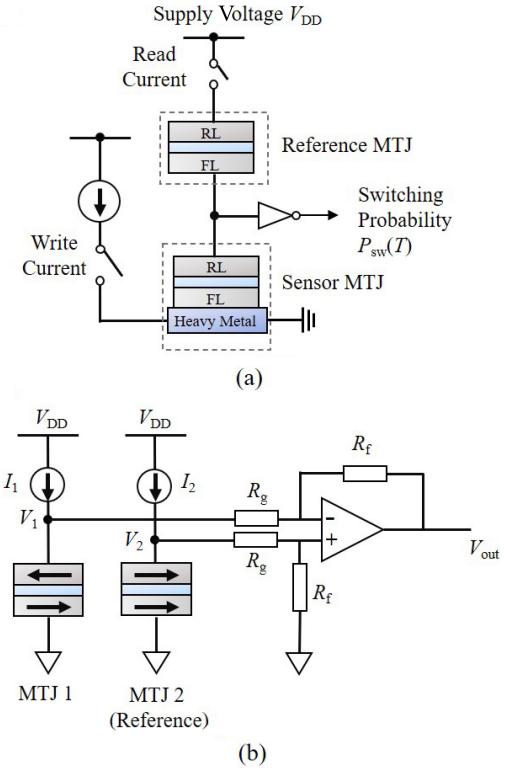

Fig. 10 Schematic of thermal sensors based on MTJs.

The dependence of anti-parallel conductance (G_{AP}) on temperature is used in another MTJ-based temperature sensor[68]. Figure 10b illustrates the principle of this sensor. The MTJ is set in the anti-parallel state, the reference one is in the parallel state. The voltage at the output terminal can directly reflect the temperature variation as the G_{AP} of MTJ increases monotonically with increasing temperature. The circuit used a differential amplifier to amplify the signal and cancel out other variations in MTJs. This temperature sensor has sufficient linear sensitivity and is ten times faster than the transit speed of a traditional thermal sensor. Besides, it can also help regulate the supply voltage of power drive ICs, extending their lifetime and improving their reliability.

5 Conclusion

This study examines the commonly used design and fabrication methods of TMR sensors. The sensor performance improvement is discussed in terms of sensitivity and noise level. Several promising applications in biomedical detection, current sensing, and temperature monitoring are illustrated. Material optimization will improve the signal to noise of the TMR sensor in the future. The cost of the TMR sensor is also expected to decrease as the market volume grows. Therefore, the TMR sensor has the potential to play a significant role in the magnetic sensing domain.

Acknowledgment

This work was financially supported by Beijing Municipal Science and Technology Project (No. Z201100004220002), the International Collaboration Project B16001, the Key Research and Development Program of Shandong Province of China (No. 2020S020201-01621), and the Magnetic Sensor Innovation Platform from Laoshan District.

References

[1] X. Y. Liu, K. H. Lam, K. Zhu, C. Zheng, X. Li, Y. M. Du, C. H. Liu, and P. W. T. Pong, Overview of spintronic sensors with Internet of Things for smart living, *IEEE Trans. Magn.*, vol. 55, no. 11, p. 0800222, 2019.

[2] R. S. Popovic, P. M. Drljaca, and C. Schott, Bridging the gap between AMR, GMR, and Hall magnetic sensors, in *Proc. 23rd Int. Conf. Microelectronics*, Nis, Yugoslavia, 2002, pp. 55–58.

[3] W. Thomson, XIX. On the electro-dynamic qualities of metals: Effects of magnetization on the electric conductivity of nickel and of iron, *Proc. Roy. Soc. Lond.*, vol. 8, pp. 546–550, 1857.

[4] R. Hunt, A magnetoresistive readout transducer, *IEEE Trans. Magn.*, vol. 7, no. 1, pp. 150–154, 1971.

[5] J. M. Daughton, Magnetoresistive memory technology, *Thin Solid Films*, vol. 216, no. 1, pp. 162–168, 1992.

[6] W. Su, Z. G. Wang, T. Wen, Z. Q. Hu, J. G. Wu, Z. Y. Zhou, and M. Liu, Linear anisotropic magnetoresistive sensor without Barber-pole electrodes, *IEEE Electr. Device Lett.*, vol. 40, no. 6, pp. 969–972, 2019.

[7] M. N. Baibich, J. M. Broto, A. Fert, F. N. Van Dau, F. Petroff, P. Etienne, G. Creuzet, A. Friederich, and J. Chazelas, Giant magnetoresistance of (001)Fe/(001)Cr magnetic superlattices, *Phys. Rev. Lett.*, vol. 61, no. 21, pp. 2472–2475, 1988.

[8] G. Binasch, P. Grünberg, F. Saurenbach, and W. Zinn, Enhanced magnetoresistance in layered magnetic structures with antiferromagnetic interlayer exchange, *Phys. Rev. B*, vol. 39, no. 7, pp. 4828–4830, 1989.

[9] B. Dieny, V. S. Speriosu, S. S. P. Parkin, B. A. Gurney, D. R. Wilhoit, and D. Mauri, Giant magnetoresistive in soft ferromagnetic multilayers, *Phys. Rev. B*, vol. 43, no. 1, pp. 1297–1300, 1991.

[10] T. Miyazaki and N. Tezuka, Giant magnetic tunneling effect in Fe/Al_2O_3/Fe junction, *J. Magn. Magn. Mater.*, vol. 139, no. 3, pp. L231–L234, 1995.

[11] D. D. Djayaprawira, K. Tsunekawa, M. Nagai, H. Maehara, S. Yamagata, N. Watanabe, S. Yuasa, Y. Suzuki, and K. Ando, 230% room-temperature magnetoresistance in CoFeB/MgO/CoFeB magnetic tunnel junctions, *Appl. Phys. Lett.*, vol. 86, no. 9, p. 092502, 2005.

[12] C. Zheng, K. Zhu, S. C. de Freitas, J. Y. Chang, J. E. Davies, P. Eames, P. P. Freitas, O. Kazakova, C. Kim, C. W. Leung, et al., Magnetoresistive sensor development roadmap (non-recording applications), *IEEE Trans. Magn.*, vol. 55, no. 4, p. 0800130, 2019.

[13] P. P. Freitas, R. Ferreira, and S. Cardoso, Spintronic sensors, *Proc. IEEE*, vol. 104, no. 10, pp. 1894–1918, 2016.

[14] R. C. Chaves, S. Cardoso, R. Ferreira, and P. P. Freitas, Low aspect ratio micron size tunnel magnetoresistance sensors with permanent magnet biasing integrated in the top lead, *J. Appl. Phys.*, vol. 109, no. 7, p. 07E506, 2011.

[15] A. V. Silva, D. C. Leitao, J. Valadeiro, J. Amaral, P. P. Freitas, and S. Cardoso, Linearization strategies for high sensitivity magnetoresistive sensors, *Eur. Phys. J. Appl. Phys.*, vol. 72, no. 1, p. 10601, 2015.

[16] P. Wiśniowski, J. M. Almeida, S. Cardoso, N. P. Barradas, and P. P. Freitas, Effect of free layer thickness and shape anisotropy on the transfer curves of MgO magnetic tunnel junctions, *J. Appl. Phys.*, vol. 103, no. 7, p. 07A910, 2008.

[17] R. Ferreira, E. Paz, P. P. Freitas, J. Wang, and S. Xue, Large area and low aspect ratio linear magnetic tunnel junctions with a soft-pinned sensing layer, *IEEE Trans. Magn.*, vol. 48, no. 11, pp. 3719–3722, 2012.

[18] T. Nakano, M. Oogane, T. Furuichi, and Y. Ando, Magnetic tunnel junctions using perpendicularly magnetized synthetic antiferromagnetic reference layer for wide-dynamic-range magnetic sensors, *Appl. Phys. Lett.*, vol. 110, p. 012401, 2017.

[19] Z. Q. Cao, W. B. Chen, S. Y. Lu, S. H. Yan, Y. Zhang, Z. T. Zhou, Y. D. Yang, Z. Li, W. S. Zhao, and Q. W. Leng, Tuning the linear field range of tunnel magnetoresistive

sensor with MgO capping in perpendicular pinned double-interface CoFeB/MgO structure, *Appl. Phys. Lett.*, vol. 118, p. 122402, 2021.

[20] L. Yuan, S. H. Liou, and D. X. Wang, Temperature dependence of magnetoresistance in magnetic tunnel junctions with different free layer structures, *Phys. Rev. B*, vol. 73, no. 13, p. 134403, 2006.

[21] C. Reig, S. Cardoso, and S. C. Mukhopadhyay, *Giant Magnetoresistance* (*GMR*) *Sensors*: *From Basis to State-of-the-Art Applications*. Berlin, Germany: Springer-Verlag, 2013.

[22] F. Franco, M. Silca, S. Cardoso, and P. P. Freitas, Optimization of asymmetric reference structures through non-evenly layered synthetic antiferromagnet for full bridge magnetic sensors based on CoFeB/MgO/CoFeB, *Appl. Phys. Lett.*, vol. 118, p. 072401, 2021.

[23] M. D. Cubells-Beltran, C. Reig, D. R. Munoz, S. I. P. C. de Freitas, and P. J. P. de Freitas, Full Wheatstone bridge spin-valve based sensors for IC currents monitoring, *IEEE Sens. J.*, vol. 9, no. 12, pp. 1756–1762, 2009.

[24] I. Berthold, M. Müller, S. Klötzer, R. Ebert, S. Thomas, P. Matthes, M. Albrecht, and H. Exner, Investigation of selective realignment of the preferred magnetic direction in spin-valve layer stacks using laser radiation, *Appl. Surf. Sci.*, vol. 302, pp. 159–162, 2014.

[25] S. H. Yan, Z. Q. Cao, Z. X. Guo, Z. Y. Zheng, A. N. Cao, Y. Qi, Q. W. Leng, and W. S. Zhao, Design and fabrication of full wheatstone-bridge-based angular GMR sensors, *Sensors*, vol. 18, p. 1832, 2018.

[26] Z. Q. Cao, Y. M. Wei, W. J. Chen, S. H. Yan, L. Lin, Z. Li, L. Z. Wang, H. W. Yang, Q. W. Leng, and W. S. Zhao, Tuning the pinning direction of giant magnetoresistive sensor by post annealing process, *Sci. China Inform. Sci.*, vol. 64, p. 162402, 2021.

[27] J. G. Deak, Practical Tunneling magnetoresistive *Z*-axis sensors, in *Proc. AMA Conf.*, Nuremberg, Germany, 2015, pp. 245–250.

[28] Z. H. Jin, M. A. I. Mohd Noor Sam, M. Oogane, and Y. Ando, Serial MTJ-based TMR sensors in bridge configuration for detection of fractured steel bar in magnetic flux leakage testing, *Sensors*, vol. 21, no. 2, p. 668, 2021.

[29] D. X. Wang, C. Nordman, J. M. Daughton, Z. H. Qian, and J. Fink, 70% TMR at room temperature for SDT sandwich junctions with CoFeB as free and reference layers, *IEEE Trans. Magn.*, vol. 40, no. 4, pp. 2269–2271, 2004.

[30] S. S. P. Parkin, C. Kaiser, A. Panchula, P. M. Rice, B. Hughes, M. Samant, and S. H. Yang, Giant tunnelling magnetoresistance at room temperature with MgO (100) tunnel barriers, *Nat. Mater.*, vol. 3, pp. 862–867, 2004.

[31] Y. M. Lee, J. Hayakawa, S. Ikeda, F. Matsukura, and H. Ohno, Effect of electrode composition on the tunnel magnetoresistance of pseudo-spin-valve magnetic tunnel junction with a MgO tunnel barrier, *Appl. Phys. Lett.*, vol. 90, p. 212507, 2007.

[32] N. Kudo, M. Oogane, M. Tsunoda, and Y. Ando, Polycrystalline $Co_2Fe_{0.4}Mn_{0.6}Si$ Heusler alloy thin films with high B2 ordering and small magnetic anisotropy for magnetic tunnel junction based sensors, *AIP Adv.*, vol. 9, p. 125036, 2019.

[33] J. P. Valadeiro, J. Amaral, D. C. Leitão, R. Ferreira, S. F. Cardoso, and P. J. P. Freitas, Strategies for pTesla field detection using magnetoresistive sensors with a soft-pinned sensing layer, *IEEE Trans. Magn.*, vol. 51, no. 1, p. 4400204, 2015.

[34] Z. Q. Lei, G. J. Li, W. F. Egelhoff, P. T. Lai, and P. W. T. Pong, Review of noise sources in magnetic tunnel junction sensors, *IEEE Trans. Magn.*, vol. 47, no. 3, pp. 602–612, 2011.

[35] W. F. Egelhoff Jr, P. W. T. Pong, J. Unguris, R. D. McMichael, E. R. Nowak, A. S. Edelstein, J. E. Burnette, and G. A. Fischer, Critical challenges for picoTesla magnetic-tunnel-junction sensors, *Sensor. Actuat. A*: *Phys.*, vol. 155, no. 2, pp. 217–225, 2009.

[36] H. Nyquist, Thermal agitation of electric charge in conductors, *Phys. Rev.*, vol. 32, no. 1, pp. 110–113, 1928.

[37] J. B. Johnson, Thermal agitation of electricity in conductors, *Phys. Rev.*, vol. 32, no. 1, pp. 97–109, 1928.

[38] S. Ingvarsson, G. Xiao, S. S. P. Parkin, W. J. Gallagher, G. Grinstein, and R. H. Koch, Low-frequency magnetic noise in micron-scale magnetic tunnel junctions, *Phys. Rev. Lett.*, vol. 85, no. 15, pp. 3289–3292, 2000.

[39] N. Smith and P. Arnett, White-noise magnetization fluctuations in magnetoresistive heads, *Appl. Phys. Lett.*, vol. 78, no. 10, pp. 1448–1450, 2001.

[40] J. S. Moodera, L. R. Kinder, T. M. Wong, and R. Meservey, Large magnetoresistance at room temperature in ferromagnetic thin film tunnel junctions, *Phys. Rev. Lett.*, vol. 74, no. 16, pp. 3273–3276, 1995.

[41] E. R. Nowak, M. B. Weissman, and S. S. P. Parkin, Electrical noise in hysteretic ferromagnet-insulator-ferromagnet tunnel junctions, *Appl. Phys. Lett.*, vol. 74, no. 4, pp. 600–602, 1999.

[42] J. M. Almeida, P. Wisniowski, and P. P. Freitas, Low-frequency noise in MgO magnetic tunnel junctions: Hooge's parameter dependence on bias voltage, *IEEE Trans. Magn.*, vol. 44, no. 11, pp. 2569–2572, 2008.

[43] R. Guerrero, M. Pannetier-Lecoeur, C. Fermon, S. Cardoso, R. Ferreira, and P. P. Freitas, Low frequency noise in arrays of magnetic tunnel junctions connected in series and parallel, *J. Appl. Phys.*, vol. 105, no. 11, p. 113922, 2009.

[44] A. S. Edelstein, G. A. Fischer, M. Pedersen, E. R. Nowak, S. F. Cheng, and C. A. Nordman, Progress toward a thousandfold reduction in $1/f$ noise in magnetic sensors using an ac microelectromechanical system flux concentrator (invited), *J. Appl. Phys.*, vol. 99, no. 8, p. 08B317, 2006.

[45] Y. S. Cui, B. Khodadadi, S. Schäfer, T. Mewes, J. W. Lu, and S. A. Wolf, Interfacial perpendicular magnetic anisotropy and damping parameter in ultra thin Co_2FeAl films, *Appl. Phys. Lett.*, vol. 102, no. 16, p. 162403, 2013.

[46] Y. C. Zhou, Low noise dual free-layer magnetoresistive sensor with coupled resonance, *J. Appl. Phys.*, vol. 105, no. 7, p. 07B708, 2009.

[47] P. Wisniowski, M. Dąbek, W. Skowronski, T. Stobiecki, S. Cardoso, and P. P. Freitas, Reduction of low frequency magnetic noise by voltage-induced magnetic anisotropy modulation in tunneling magnetoresistance sensors, *Appl. Phys. Lett.*, vol. 105, p. 082404, 2014.

[48] B. Dieny, I. L. Prejbeanu, K. Garello, P. Gambardella, P. Freitas, R. Lehndorff, W. Raberg, U. Ebels, S. O. Demokritov, J. Akerman, et al., Opportunities and challenges for spintronics in the microelectronics industry, *Nat. Electron.*, vol. 3, no. 8, pp. 446–459, 2020.

[49] P. P. Sharma, E. Albisetti, M. Massetti, M. Scolari, C. La Torre, M. Monticelli, M. Leone, F. Damin, G. Gervasoni, G. Ferrari, et al., Integrated platform for detecting pathogenic DNA via magnetic tunneling junction-based biosensors, *Sensor. Actuat. B: Chem.*, vol. 242, pp. 280–287, 2017.

[50] D. Q. Su, K. Wu, R. Saha, C. Y. Peng, and J. P. Wang, Advances in magnetoresistive biosensors, *Micromachines*, vol. 11, no. 1, p. 34, 2020.

[51] M. L. Wang, Y. Wang, L. Peng, and C. F. Ye, Measurement of triaxial magnetocardiography using high sensitivity tunnel magnetoresistance sensor, *IEEE Sens. J.*, vol. 19, no. 21, pp. 9610–9615, 2019.

[52] K. Fujiwara, M. Oogane, A. Kanno, M. Imada, J. Jono, T. Terauchi, T. Okuno, Y. Aritomi, M. Morikawa, M. Tsuchida, et al., Magnetocardiography and magnetoencephalography measurements at room temperature using tunnel magnetoresistance sensors, *Appl. Phys. Express*, vol. 11, no. 2, p. 023001, 2018.

[53] D. Moretti, M. L. DiFrancesco, P. P. Sharma, S. Dante, E. Albisetti, M. Monticelli, R. Bertacco, D. Petti, P. Baldelli, and F. Benfenati, Biocompatibility of a magnetic tunnel junction sensor array for the detection of neuronal signals in culture, *Front. Neurosci.*, vol. 12, p. 909, 2018.

[54] J. Y. Chen, Y. C. Lau, J. M. D. Coey, M. Li, and J. P. Wang, High performance MgO-barrier magnetic tunnel junctions for flexible and wearable spintronic applications, *Sci. Rep.*, vol. 7, p. 42001, 2017.

[55] L. M. Loong, W. Lee, X. P. Qiu, P. Yang, H. Kawai, M. Saeys, J. H. Ahn, and H. Yang, Flexible MgO barrier magnetic tunnel junctions, *Adv. Mater.*, vol. 28, no. 25, pp. 4983–4990, 2016.

[56] A. Tanwear, X. P. Liang, Y. C. Liu, A. Vuckovic, R. Ghannam, T. Bohnert, E. Paz, P. P. Freitas, R. Ferreira, and H. Heidari, Spintronic sensors based on magnetic tunnel junctions for wireless eye movement gesture control, *IEEE Trans. Biomed. Circuits Syst.*, vol. 14, no. 6, pp. 1299–1310, 2020.

[57] G. S. Cañón Bermúdez, H. Fuchs, L. Bischoff, J. Fassbender, and D. Makarov, Electronic-skin compasses for geomagnetic field-driven artificial magnetoreception and interactive electronics, *Nat. Electron.*, vol. 1, pp. 589–595, 2018.

[58] Z. P. Song, Z. C. Cao, Z. J. Li, J. L. Wang, and Y. H. Liu, Inertial motion tracking on mobile and wearable devices: Recent advancements and challenges, *Tsinghua Science and Technology*, vo. 26, no. 5, pp. 692–705, 2021.

[59] J. S. Donnal and S. B. Leeb, Noncontact power meter, *IEEE Sens. J.*, vol. 15, no. 2, pp. 1161–1169, 2015.

[60] E. G. Vidal, D. R. Muñoz, S. I. R. Arias, J. S. Moreno, S. Cardoso, R. Ferreira, and P. Freitas, Electronic energy meter based on a tunnel magnetoresistive effect (TMR) current sensor, *Materials*, vol. 10, no. 10, p. 1134, 2017.

[61] X. Sun, Q. Huang, Y. H. Hou, L. J. Jiang, and P. W. T. Pong, Noncontact operation-state monitoring technology based on magnetic-field sensing for overhead high-voltage transmission lines, *IEEE Trans. Power Deliv.*, vol. 28, no. 4, pp. 2145–2153, 2013.

[62] X. Sun, W. K. Lee, Y. H. Hou, and P. W. T. Pong, Underground power cable detection and inspection technology based on magnetic field sensing at ground surface level, *IEEE Trans. Magn.*, vol. 50, no. 7, p. 6200605, 2014.

[63] L. S. Rosado, F. A. Cardoso, S. Cardoso, P. M. Ramos, P. P. Freitas, and M. Piedade, Eddy currents testing probe with magneto-resistive sensors and differential measurement, *Sensor. Actuat. A*: *Phys.*, vol. 212, pp. 58–67, 2014.

[64] Y. H. Bai, C. F. Ye, X. C. Tao, N. Zhang, and X. G. Li, Magnetic imaging of sludge outside steam generator tube with array magnetoresistance sensors, *IEEE Sens. J.*, vol. 21, no. 6, pp. 7439–7448, 2021.

[65] C. F. Ye, Y. Wang, and Y. Tao, High-density large-scale TMR sensor array for magnetic field imaging, *IEEE Trans. Instrum. Meas.*, vol. 68, no. 7, pp. 2594–2601, 2019.

[66] N. Maciel, E. Marques, L. Naviner, Y. L. Zhou, and H. Cai, Magnetic tunnel junction applications, *Sensors*, vol. 20, no. 1, p. 121, 2020.

[67] A. Sengupta, C. M. Liyanagedera, B. Jung, and K. Roy, Magnetic tunnel junction as an on-chip temperature sensor, *Sci. Rep.*, vol. 7, no. 1, p. 11764, 2017.

[68] Y. F. Jiang, Y. S. Zhang, A. Klemm, and J. P. Wang, Fast spintronic thermal sensor for IC power driver cooling down, in *Proc.2016 IEEE Int. Electron Devices Meeting*, San Francisco, CA, USA, 2016, pp. 26.2.1–26.2.4.

Shaohua Yan received the BS degree in information and computing science and the MS degree in electronic science and technology from Beihang University, China, in 2015 and in 2018, respectively, where she is currently pursuing the PhD degree in microelectronics and solidstateelectronics. Her research interests mainly include the design and fabrication of magnetoresistance sensors.

Zitong Zhou received the BS degree in microelectronics science and engineering from Hubei University, China in 2017. She is currently pursuing the PhD degree in microelectronics and solid state electronics at Beihang University. Her research interests mainly include the noise performance of the magnetoresistance sensors.

Yaodi Yang received the BS degree in chemical and physical science from the University of Toronto, Canada in 2020. He is currently interning in the Beihang-Goertek Joint Microelectronics Institute at Qingdao Research Institute of Beihang University.

Qunwen Leng received the MS degree in solid state physics from the Institute of Physics, Chinese Academy of Sciences, in 1988, and the PhD degree in physics from the University of Cologne, in 1994. He is currently the vice president of Goertek Inc., the vice dean of the Beihang-Goertek Joint Microelectronics Institute, and a professor at Beihang University. His research interests include the GMR and TMR sensors

Weisheng Zhao received the PhD degree in physics from the University of Paris-Sud, France, in 2007. He was nominated as tenured research scientist at CNRS, Grenoble, France, in 2007. In 2013, he joined Beihang University, Beijing, China, where he is currently the dean of School of Integrated Circuit Science and Engineering. He has authored or coauthored more than 200 scientific articles, including *Advanced Materials*, *Nature Communications*, and *IEEE Transactions*. His research interests include the new non-volatile memory (spin transfer torque and spin orbit torque MRAM), circuit design, and magnetoresistance sensors.